04

Molecules of 2-methylbenzimidazole perchlorate $C_8H_8N_2-HClO_4$ in borate glass nanopores: X-ray and dielectric studies

© A.A. Levin, A.V. Fokin, E.V. Balashova, B.B. Krichevtsov

Ioffe Institute,
St. Petersburg, Russia

E-mail: aleksandr.a.levin@mail.ioffe.ru

Received April 30, 2025
Revised September 11, 2025
Accepted November 11, 2025

New semi-organic nanostructures were synthesized by introducing 2-methylbenzimidazole perchlorate ($MBI-HClO_4$) molecules into porous borate glasses with pore sizes of ~ 3 and ~ 7 nm. X-ray diffraction studies have shown that the nanostructures contain several phases with the $MBI-HClO_4$ crystal structure, but slightly different lattice parameters. In some phases, as a result of the random orientation of the pores of the glasses, crystallites larger than the pore sizes are formed. The temperature and frequency dependences of capacitance, $\mathrm{tg}\,\delta$, and conductivity were measured for the obtained nanostructures. The results of the analysis of dielectric properties by methods of dielectric spectroscopy are presented.

Keywords: nanostructures, crystal structure, X-ray diffraction, dielectric properties, dielectric spectroscopy.

DOI: 10.61011/PSS.2025.12.63091.7954k-25

1. Introduction

Currently, much attention is being paid to the development and study of new nanostructures (NS) that can be used as functional materials in microelectronics, energy, biomedicine, and other fields [1,2]. One of the promising directions for creating such NS is the use of porous nanomatrices, the nanoscale pores of which can be filled with substances with various properties — magnetic, ferroelectric, piezoelectric, superconducting, bioactive, etc. Borate glasses, chrysotile asbestos, and mesoporous silicon can act as nanomatrices [3].

Earlier [4], we have synthesized NS in which 2-methylbenzimidazole ($C_8H_8N_2$, MBI) was used as a filler for the pores of borate glasses, chrysotile asbestos, and mesoporous silicon, the crystals of which have ferroelectric properties above room temperature (RT) [5]. MBI molecules easily penetrate into the pores of glasses, chrysotile asbestos filaments, and, as X-ray diffraction (XRD) studies have shown, their entry is accompanied by the appearance of MBI phases with close unit cell parameters but very different crystallite sizes. In addition, the introduction of MBI is accompanied by strong changes in the optical and dielectric properties of NS compared to unfilled matrices [4].

Recently, we have synthesized a new crystal, 2-methylbenzimidazole perchlorate ($MBI-HClO_4$), based on a combination of MBI and perchloric acid ($HClO_4$) [6]. At room temperature, $MBI-HClO_4$ crystallizes in the space group (sp. gr.) $P2_1/n$ (14), and when the temperature T increases, it undergoes two phase transitions of the first order [6]: first to an intermediate state at $T_{LC} = 161.3\,^\circ C$ demonstrating the properties of a liquid crystal (LC), and then into the liquid state (LS) at $T_{melt} = 168.4\,^\circ C$. Upon cooling, phase transitions occur at lower temperatures. As shown by dielectric and optical studies of $MBI-HClO_4$ crystals and films [6,7], during the transition to optically isotropic LC, the conductivity increases by 5–7 orders of magnitude compared to RT, which indicates [8,9] that an ionic liquid (IL) is formed in this phase. The conductivity of $MBI-HClO_4$ in the LC state is about two orders of magnitude higher than in the low-temperature crystalline state, which indicates [10] the possibility of the formation of an ionic liquid crystal (ILC) in this phase. It seemed interesting to synthesize NS based on $MBI-HClO_4$ and see how the giant changes in the conductivity of $MBI-HClO_4$ during phase transitions would affect the dielectric properties of the NS. A prerequisite for such work was to obtain evidence of the presence of the $MBI-HClO_4$ phase in the matrix of nanocrystals (NC) and to estimate the size of its crystallites. As studies of NS based on MBI have shown, this is possible using XRD methods [6]. The aim of the work was to prepare NS in the form of borate glasses filled with $MBI-HClO_4$ molecules, study their crystal structure, and conduct dielectric studies in the temperature range, including the state of the IL.

NS were produced by placing borate glass samples with pore diameters of ~ 3 and ~ 7 nm in a melt of $MBI-HClO_4$ crystals. Glasses with such pore sizes were previously used by us when producing NS based on MBI [4]. It was of interest to obtain such NS based on $MBI-HClO_4$. The $MBI-HClO_4$ crystals themselves were grown by slow cooling of an aqueous solution of pre-purified MBI crystals and perchloric acid. No external pressure is required to fill the pores with $MBI-HClO_4$ molecules, since they enter the pores of borate glasses from the liquid due to osmotic pressure. After extracting the

samples from the melt, the plane-parallel faces of the filled borate glasses were thoroughly cleaned mechanically. As shown by experiments with weighing samples before and after synthesis, the filling degree was ∼ 70, 80, and 90 % for samples with pore diameters of ∼ 3 and ∼ 7 nm, hereinafter referred to as S3nm-70, S3nm-80, and S7nm-90.

The XRD measurements of the samples were carried out using $\theta - 2\theta$ scan mode on a D2 Phaser X-ray diffractometer (Bruker AXS, Karlsruhe, Germany), designed in a vertical Bragg–Brentano θ/θ scheme and equipped with a linear LYNXEYE semiconductor detector (Bruker AXS) for registration of the XRD signal. Cu-K_α radiation from an X-ray tube with a copper anode filtered by a Ni filter absorbing Cu-K_β radiation was used. The temperature in the sample chamber during measurements was 314 ± 2 K. To determine angular corrections to the obtained XRD patterns, additional measurements were performed on samples immersed flush with the surface of NaCl powder, the Bragg reflection angles of which are calibrated using a standard Si640f powder sample (NIST, Gaithersburg, MD, USA). For preliminary analysis in order to obtain optimal initial parameter values for the Rietveld method, one used the programs Celsiz (to calculate unit cell parameters based on Bragg angles after the angular corrections and Miller indices of the reflections) and SizeCr (to estimate the mean crystallite size D and the absolute value of the mean microstrain ε_s using the Williamson–Hall plot (WHP) and size-strain plot (SSP) methods, taking into account the type of reflections). The data obtained as a result of the preliminary analysis were used as a starting point for the analysis of the XRD patterns by the Rietveld method using the TOPAS program (version 5, Bruker AXS) in order to obtain accurate values of these values. All necessary descriptions of programs and methods can be found in [4].

To conduct dielectric studies, electrodes made of thin aluminum foil were applied to the cleaned plane-parallel faces of filled borate glasses. Capacitance C and $\mathrm{tg}\,\delta$ were measured on the samples in the frequency range $f = 25-106$ Hz and the temperature range 295–460 K using MIT 9216A LCR-meters (Protek Instrument Co., Ltd., Gyeonggi, Republic of Korea) and E7-20 (MNIPI, Minsk, Belarus).

X-ray phase analysis of the XRD patterns of the samples showed that all the observed reflections with well–resolved profiles can be attributed to phases Ph1 and Ph2 characterized by the MBI–$HClO_4$ structure, but with slightly different unit cell parameters. Judging by the magnitude of the full width at half of the maximum FWHM of the observed reflections, the crystallites of these phases differ markedly (the Ph1 phase has larger crystallite sizes than the Ph2 phase). Based on the criterion $\mathrm{FWHM}/B_{\mathrm{int}} = 0.70(7)-0.81(11)$, where B_{int} is the whole integral width of the reflection, the reflections of both phases are attributed to the pseudo-Voigt (pV) type. As an example, Figure 1 shows a graph constructed by the SSP method for the S3nm-70 sample. Tables 1 and 2 show the data obtained using the Celsiz program and the

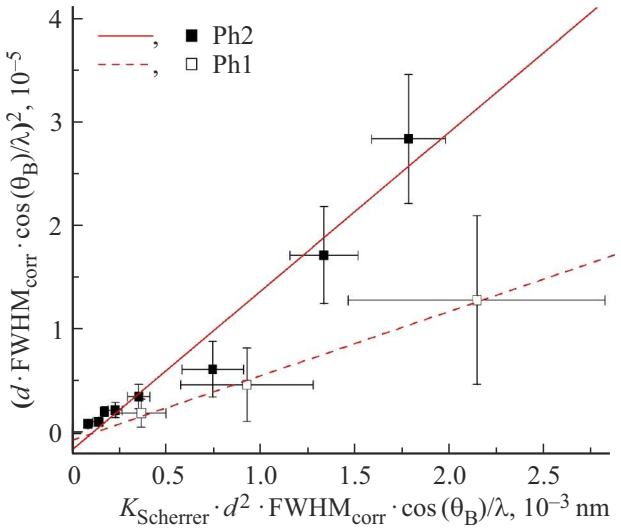

Figure 1. SSP for phases Ph1 and Ph2 of the S3nm-70 sample. θ_B is half the Bragg angle $2\theta_B$ of the reflection after applying angular corrections and d is the interplane distance in nm corresponding to the Bragg angle $2\theta_B$; $\mathrm{FWHM_{corr}}$ is the FWHM of the reflection corrected to instrumental broadening according to the procedure for the observed pV type of reflections; $\lambda = 0.1590598$ nm is the wavelength of Cu-$K_{\alpha 1}$ radiation after correction of the contribution of Cu-$K_{\alpha 2}$; the other designations are explained in Table 1. Approximating lines $Y = A + B \cdot X$ are drawn, where the expressions for X and Y are given on the abscissa and ordinate axes, respectively. For both phases $A < 0$, which means that there is no microstrain ($\varepsilon_s = 0$).

WHP and SSP methods for all samples; here and further, in round parentheses after the given values, their estimated standard deviations (e.s.d.s) are given. When calculating WHP and SSP, the values of the coefficients of the Scherrer and Wilson-Stokes equations $K_{\mathrm{Scherrer}} = 0.94$ and $K_{\mathrm{strain}} = 4$, respectively, were used. Since the determination coefficient R_{cod} in SSP, unlike WHP, is greater than 90 %, the SSP method gives reliable results, confirming the results of WHP. The MBI–$HClO_4$ structure model from [6] was used to refine the parameters of the Ph1 and Ph2 phases using the Rietveld method. The parameters of the unit cell and the isotropic temperature factors B_{iso} of atoms, common to atoms of the same sort, were refined; the coordinates of the atoms were not refined. It was assumed that the B_{iso} of the atoms of phase Ph1 (and Ph3, which are discussed below) the same as in the Ph2 phase, to which most of the observed reflections belong. In addition to the background in the form of a seventh-order Chebyshev polynomial with an additional hyperbolic function for $2\theta < 11°$, the parameters of two amorphous porous glass halos defined by asymmetric Pearson VII (SPVII) functions centered at 2θ angles of approximately 22.35° and 78.56° were refined. As in [4] for MBI in borate glasses, during the final refinement cycles in the two-phase model, the presence of a third phase (Ph3 phase) with small crystallite sizes approximately equal to the pore diameter was assumed,

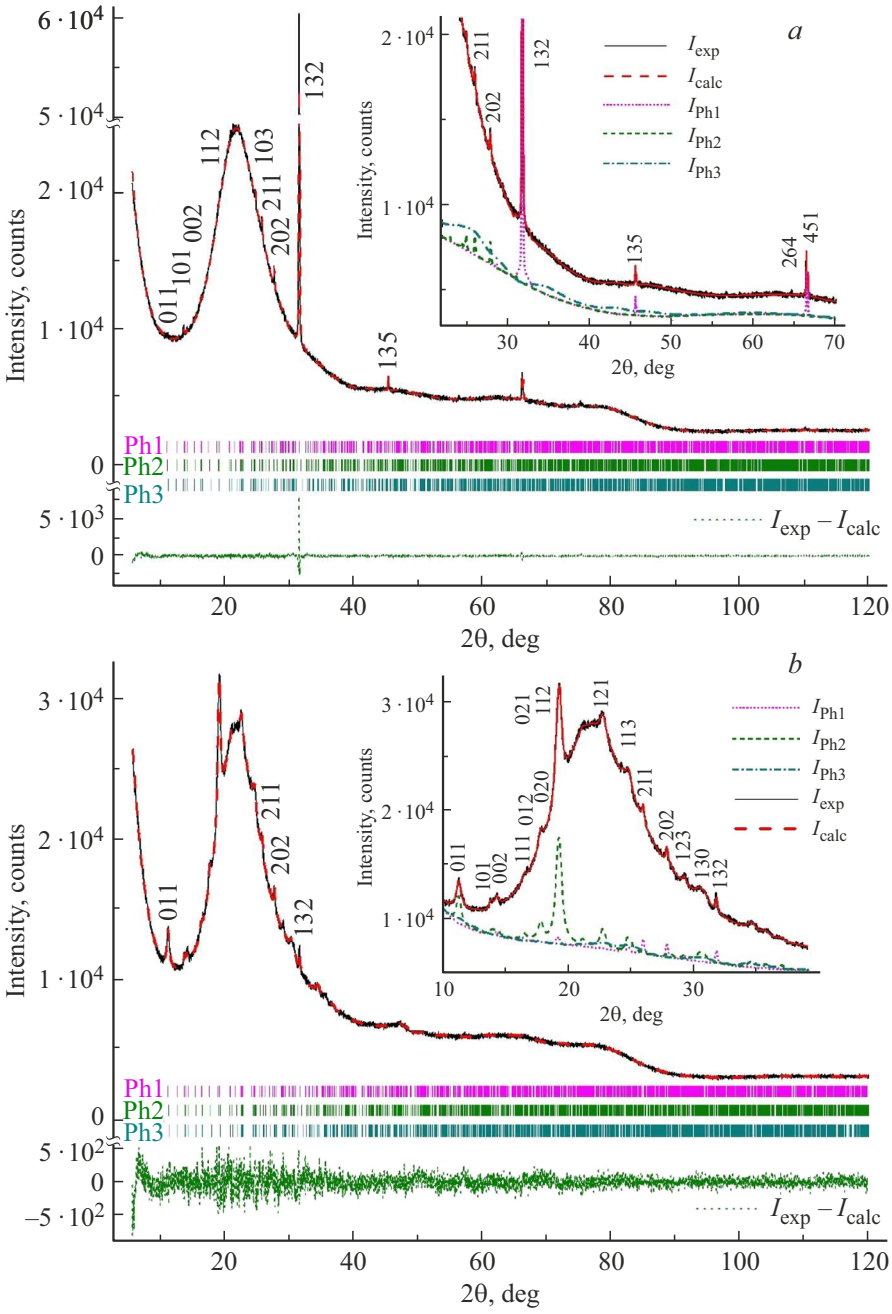

Figure 2. Results of the analysis of XRD patterns of samples (*a*) S3nm-70 and (*b*) S7nm-90 by the Rietveld method. Angular positions (Bragg angles) corresponding to the refined unit cell parameters (Table 3) are shown by vertical dashes under the XRD patterns. The inserts show in an enlarged scale the angular ranges of XRD-patterns, in which most reflections with a clearly distinguishable profile are observed. The Miller indices *hkl* of selected reflections are indicated.

the reflections of which are clearly not resolved in the XRD patterns of the samples against the background of a large amorphous halo from the glass. Since the changes in the weighted profile agreement factor R_{wp} upon the introduction of the Ph3 phase were small (a decrease of only $\sim 0.2-0.4\,\%$) due to the low intensity of reflections and the high background, tracking during the structure refinement was carried out using the weighted profile agreement factor cR_{wp} (with background subtraction), which is much more sensitive. Taking into account the preferential orientation within the framework of the March–Dollas model along two directions, different for different phases and samples, led to a decrease in cR_{wp} by $\sim 70\,\%$ for the S3nm-70 sample with sufficiently strong reflections and by ~ 5 and $\sim 13.3\,\%$, respectively, for S3nm-80 and S7nm-90 samples with weak reflections. The introduction of the Ph3 phase for these samples resulted in a decrease in cR_{wp} by ~ 4.6, ~ 14.3, and $\sim 2.8\,\%$, respectively, which is large enough to confirm

Table 1. The parameters of the monoclinic unit cell a, b, c, β and its volume V_{cell} for the crystalline phases MBI–$HClO_4$ according to the results of calculations by the program Celsiz

Phase	a, Å	b, Å	c, Å	β, °	V_{cell}, Å^3
sample S3nm-70					
Ph1	–[a]	–[a]	–[a]	–[a]	–[a]
Ph2	7.866(19)	9.966(15)	12.703(32)	95.42(6)	991.8(3.8)
sample S3nm-80					
Ph1	7.903(50)	10.053(40)	12.710(48)	95.95(24)	1004.4(8.4)
Ph2	7.908(9)	9.956(8)	12.646(8)	95.57(9)	990.9(1.5)
sample S3nm-90					
Ph1	–[a]	–[a]	–[a]	–[a]	–[a]
Ph2	7.859(23)	9.926(35)	12.741(39)	95.44(18)	989.4(5.5)

Note. [a] the value cannot be calculated because only three reflections are observed.

Table 2. The results of the preliminary XRD investigation of samples using profile analysis methods: the mean value of the FWHM/B_{int} reflection type criterion, the mean crystallite size D and the absolute mean value of the microstrain ε_s according to the results of WHP and SSP, as well as the coefficient of determination R_{cod} of the WHP and SSP graphs

Phase	FWHM/B_{int}	WHP		SSP	
		D, nm	R_{cod}, %	D, nm	R_{cod}, %
sample S3nm-70					
Ph1	0.76(8)	186(16)[a]	31.51	186(16)[a]	99.54
Ph2	0.74(3)	96(22)[a]	13.46	96(22)[a]	96.19
sample S3nm-80					
Ph1	0.80(10)	59(6)[a]	16.05	59(6)[a]	96.22
Ph2	0.70(7)	31(8)[a]	67.53	31(8)[a]	96.64
sample S3nm-90					
Ph1	0.76(14)	55(11)[a]	81.97	55(11)[a]	95.89
Ph2	0.81(11)	24(4)[b]	3.44	24(2)[b]	91.58

Note 1. [a] both methods, WHP and SSP, result in $\varepsilon_s = 0$.
Note 2. [b] both methods, WHP and SSP, result in $\varepsilon_s = 0.24(17)\,\%$.

the assumption of the presence of this phase. The final refinement results are presented in Tables 3 and 4 and in Figure 2 (for samples S3nm-70 and S7nm-90 as an example). The same values of the $K_{Scherrer}$ and K_{strain} coefficients were used as in the calculation of WHP and SSP. All the e.s.d.s of the parameters obtained during refinement are corrected for underestimation due to serial correlations by multiplying by the coefficient $m_{e.s.d.}$ calculated using the program RietEsd (see references in [4]). As can be seen from Table 4, the largest number of MBI–$HClO_4$ crystallites has a size D close to the pore diameter (93.1, 85.3, and 62.4 wt.% of the Ph3 phase for samples S3nm-70, S3nm-80, and S7nm-90, respectively). In samples S3nm-70, S3nm-80, and S7nm-90, the crystallites of the Ph1 phase with the largest sizes D, equal to ~ 235, 68, and 53 nm, respectively, show the lowest content of 2.1–3.2 wt.%. The content of the phase Ph2 with intermediate D values of ~ 94, 40, and 24 nm in these samples is 4.8, 12.1, and 34.4 wt.%, respectively. In the Ph2 phase of the S7nm-90 sample, the presence of microstrains ($\varepsilon_s \approx 0.33\,\%$), as predicted by the results of profile analysis, was confirmed. The crystallite sizes of the Ph1 and Ph2 phases obtained by refinement using the Rietveld method are in satisfactory agreement with the results of profile analysis (compare Tables 1, 2 and 3, 4)

X-ray methods in the $\theta - 2\theta$ scan mode provide information on the mean crystallite size D in the direction perpendicular to the surface on which the X-rays fall. Porous glasses have a random arrangement of pores, resulting in some sections of the pores being perpendicular or nearly perpendicular to the glass surface or at an angle relative to it, while others are parallel to it (sections 1, 2, and 3, respectively, in Figure 3). It is likely that the Ph1 phase with the largest detectable crystallite size is formed in perpendicular sections 1, the Ph2 phase with intermediate D values is formed in inclined sections 2, and the Ph3 phase with a D size approximately equal to the pore diameter is formed in parallel sections 3. It is possible that some part of the Ph2 phase is also formed in sections 1, and part of the Ph3 phase is formed in sections 1 and 2.

Table 3. The parameters of the monoclinic unit cell a, b, c, β and its volume V_{cell} for the crystalline phases MBI–$HClO_4$ according to the results of refinement by the Rietveld method

Phase	a, Å	b, Å	c, Å	β, °	V_{cell}, Å^3
sample S3nm-70					
Ph1	7.8894(7)	10.0831(2)	12.6926(7)	95.50(1)	1005.0(1)
Ph2	7.891(3)	9.965(18)	12.683(9)	95.46(3)	992.8(2.0)
Ph3	7.964(13)	9.856(16)	12.665(19)	95.72(11)	989.2(2.7)
sample S3nm-80					
Ph1	7.900(5)	10.061(5)	12.707(20)	95.89(8)	1004.6(1.8)
Ph2	7.907(3)	9.962(10)	12.658(8)	95.55(3)	992.4(1.2)
Ph3	7.967(15)	9.857(56)	12.691(20)	95.12(26)	992.7(6.2)
sample S3nm-90					
Ph1	7.905(2)	10.084(3)	12.796(18)	95.45(3)	1015.4(1.5)
Ph2	7.868(4)	9.978(2)	12.744(4)	95.55(3)	995.8(6)
Ph3	7.882(9)	9.865(30)	12.752(46)	95.62(27)	986.8(4.8)

Table 4. The results of the analysis of XRD patterns of samples using the Rietveld method: the mean size D of crystallites and the absolute average value of the microstrain ε_s, the agreement factors (the Bragg factor R_B, the weighted profile factor R_{wp}, profile factor R_p and their analogues after background subtraction, cR_{wp} and cR_p), as well as the coefficient $m_{\text{e.s.d.}}$ for correction of estimated standard deviations (e.s.d.s) of the refined parameters

Phase	W_t, wt.%	D, nm	ε_s, %	R_B, %	R_{wp}, %	R_p, %	cR_{wp}, %	cR_p, %	$m_{\text{e.s.d.}}$[a]
sample S3nm-70									
Ph1	2.13(3)	235(1)	0[b]	0.652	1.753	1.164	18.740	24.136	1.929
Ph2	4.76(4)	94(11)	0[b]	0.306					
Ph3	93.11(8)	2.7(1)	0[b]	0.123					
sample S3nm-80									
Ph1	2.6(1)	68(11)	0[b]	0.166	1.179	0.909	21.231	24.549	1.522
Ph2	12.1(3)	40.0(2.3)	0[b]	0.174					
Ph3	85.3(3)	2.8(1)	0[b]	0.101					
sample S3nm-90									
Ph1	3.2(1)	53.2(3.5)	0[b]	0.206	1.252	0.967	20.906	25.524	1.558
Ph2	34.4(5)	23.7(3)	0.326(6)[c]	0.096					
Ph3	62.4(5)	6.0(2)	0[b]	0.152					

Note 1. [a] were calculated by the program RietEsd, since the program TOPAS gives incorrect cR_{wp} and cR_p values when using a hyperbolic addition to the background, see [4].
Note 2. [b] $\varepsilon_s = 0$ was fixed based on the results of the preliminary investigation.
Note 3. [c] $\varepsilon_s(\%) = 2e_0 \cdot 100\,\%$, where e_0 is the microstrain parameter obtained by the program TOPAS during refinement, see [4].

Figures 4, *a, b* show the temperature dependences of capacitance C and $\operatorname{tg}\delta$ in borate glass with a pore diameter of ~ 3 nm, filled with MBI–$HClO_4$, at frequencies f from 120 Hz to 100 kHz. An increase in temperature leads to a significant increase in capacity. At a frequency of $f = 120$ Hz, the capacitance of the structure increases from $C \approx 20$ pF at RT to 10 nF at 430 K. As the frequency increases, these changes decrease. The temperature dependences of $\operatorname{tg}\delta$ in this temperature range show maxima that shift towards higher temperatures with increasing frequency, which is typical for the thermal activation mechanism of dielectric losses. As is known, the values of C and $C \cdot tg\delta$ are proportional, respectively, to the imaginary and real parts of the dielectric constant. Their temperature (Figures 4, *a, b*) and frequency (Figures 4, *c, d*) dependences for the investigated NS exhibit behavior characteristic of dielectric relaxation.

An increase in capacitance and conductivity by several orders of magnitude at low frequencies during the transition of the crystal to the IL state is associated with the formation of electric double layers (EDL) on the surfaces of the electrodes in contact with the IL. Methods of dielectric and impedance spectroscopy are used to study the properties of EDL and IL. Figure 4, *c* shows the frequency dependences of the capacitance C of a composite NS when a constant electric field U of various magnitudes is applied. The constant field reduces the value of C especially strongly at low frequencies in the voltage range $U = 0$–2 V. With a further increase in voltage ($U > 2$ V), no significant changes in capacitance are observed. The frequency dependences of the conductivity G have a complex character (Figure 4, *d*). In particular, at $f > 104$ Hz, a strong frequency dependence

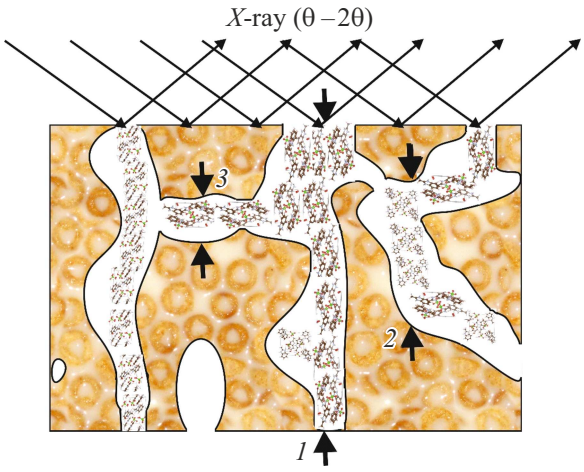

Figure 3. Schematic illustration of the formation of MBI–$HClO_4$ crystallites of different orientations and sizes in randomly oriented pores of borate glass. X-rays incident on the sample surface and diffracting X-rays in the case of $\theta - 2\theta$ scanning are indicated. The different types of pore orientation are shown by numbers *1, 2*, and *3*.

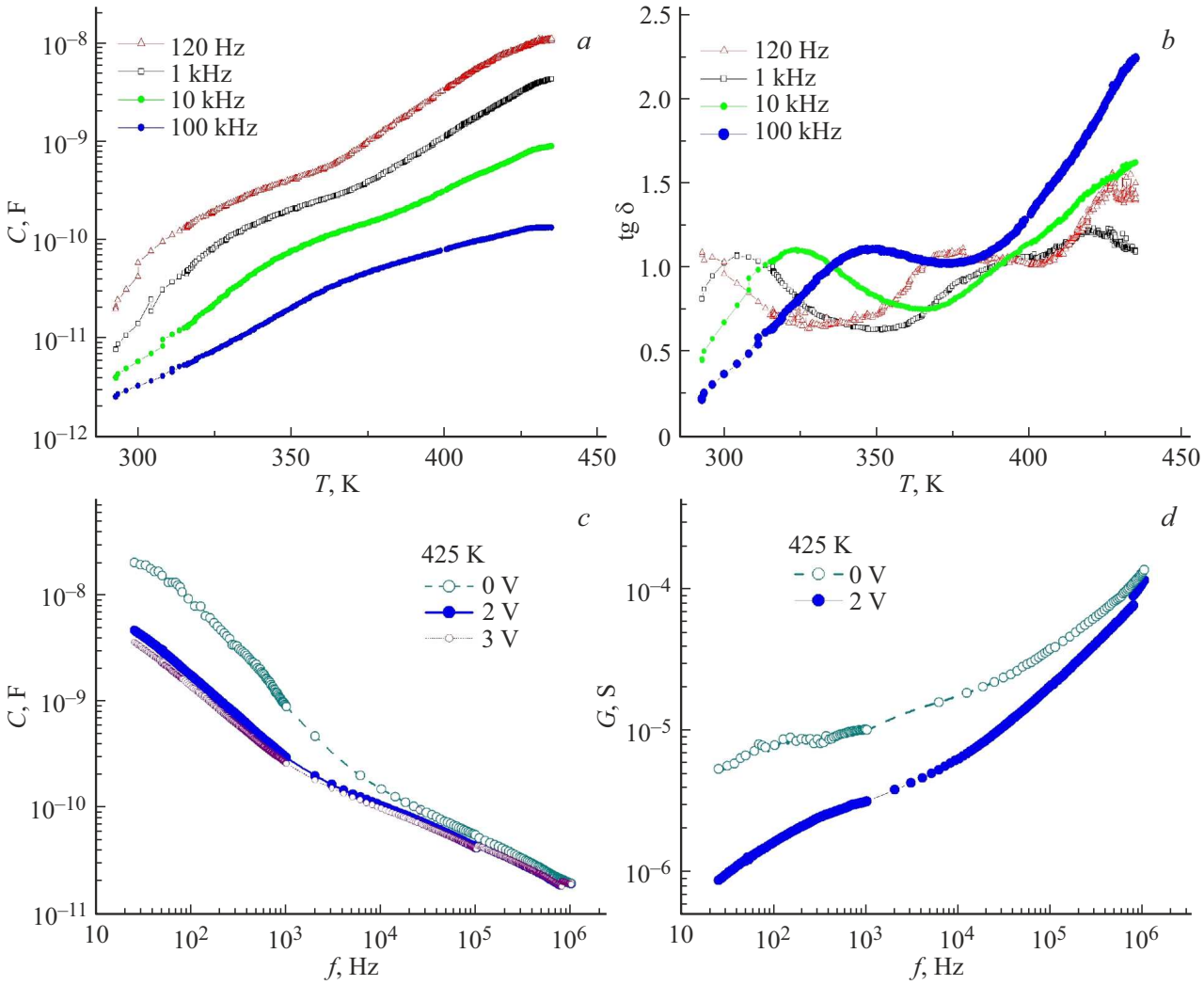

Figure 4. Borate glass with a pore diameter of 3 nm filled with MBI–$HClO_4$ (sample S3nm-70). (*a, b*) Temperature dependences of capacitance C (*a*) and $\mathrm{tg}\,\delta$ (*b*) at frequencies $f = 120$ Hz, 1 kHz, 10 kHz, and 100 kHz and (*c, d*) frequency dependences of capacitance C (*c*) and conductivity G (*d*) at a constant electric field voltage $U = 0$, 2, and 3 V.

of G is observed, while at f values in the range of 102–104 Hz, a weak frequency dependence of G is seen, indicating a significant contribution from direct current conductivity. At $f < 102$ Hz, a decrease in G is observed, associated with the formation of an EDL. Applying an electric field reduces G by approximately an order of magnitude and enhances the influence of the EDL on G.

Thus, the XRD study showed that after holding porous borate glasses in the MBI–$HClO_4$ melt, phases with the same MBI–$HClO_4$ structure, but with different, albeit close, unit cell parameters crystallize in the pores of glasses with diameters of ~ 3 and 7 nm. Due to the random arrangement of pores relative to the glass surface, crystallites of different phases are characterized by sizes ranging from comparable to the pore diameters to significantly exceeding them. As follows from the results of dielectric measurements, a significant increase in capacitance and conductivity at low frequencies indicates the transition of the NCs to the IL or ILC state. The transitions are very blurred, which indicates a large spread of transition temperatures in the NCs.

Acknowledgments

For XRD measurements and analysis, equipment and software of the Federal Center for Joint Use „Materials Science and Diagnostics in Advanced Technologies“ (Ioffe Institute, St. Petersburg, Russia) were used.

Conflict of interest

The authors declare that they have no conflict of interest.

References

[1] S. Pergher, E. Rodríguez-Castellón, Appl. Sci. **9**, 1314 (2019). DOI: 10.3390/app9071314

[2] B.H Alshammari, M.M.A. Lashin, M.A. Mahmood, F.S Al-Mubaddel, R.N. de Nasir Ilyas, M. Sohail, A. Khan, S.S. Abdullaev, R. Khan. RSC Adv. **13**, *20*, 13735 (2023). DOI: 10.1039/D3RA01421E
[3] Y. Kumzerov, S. Vakhrushev. In: Encyclopedia of Nanoscience and Nanotechnology / Ed. H.S. Nalwa. American Scientific Publishers, Los Angeles (2004). Vol. 3, p. 811.
[4] E. Balashova, A.A. Levin, A. Smirnov, V. Davydov, S. Pavlov, A. Starukhin, A. Fokin, D. Kurdyukov, D. Eurov, B. Krichevtsov. Int. J. Mol. Sci. **24**, *18*, 13740 (2023). DOI: 10.3390/ijms241813740
[5] S. Horiuchi, F. Kagawa, K. Hatahara, K. Kobayashi, R. Kumai, Y. Murakami, Y. Tokura. Nat. Commun. **3**, 1308 (2012). DOI: 10.1038/ncomms2322
[6] E. Balashova, A. Zolotarev, A.A. Levin, V. Davydov, S. Pavlov, A. Smirnov, A. Starukhin, B. Krichevtsov, H. Zhang, F. Li, H. Luo, H. Ke. Materials **16**, *5*, 1994 (2023). DOI: 10.3390/ma16051994
[7] E.V. Balashova, A.A. Levin, B.B. Krichevtsov. Techn. Phys. Lett. **50**, *12*, 157 (2024). DOI: 10.61011/TPL.2024.12.60381.6466k
[8] T. Zhou, Ch. Guid, L. Sun, Y. Hua, H. Lyu, Z. Wange, Zh. Song, G. Yu. Chem. Rev. **123**, *21*, 12170 (2023). DOI: 10.1021/acs.chemrev.3c00391
[9] Dielectric Properties of Ionic Liquids / Ed. M. Paluch. Springer International Publishing, Cham (2016). DOI: 10.1007/978-3-319-32489-0.
[10] K. Binnemans. Chem. Rev. **105**, 4148 (2005). DOI: 10.1021/cr0400919